Ignition of Aluminum Particle Clouds Behind Reflected Shock Waves

Kaushik Balakrishnan[1,*], Allen L. Kuhl[2], John B. Bell,[1] and Vincent E. Beckner[1]

[1] Lawrence Berkeley National Laboratory, 1 Cyclotron Road, Berkeley, CA 94720

[2] Lawrence Livermore National Laboratory, 7000 East Avenue, Livermore, CA 94551

Abstract

Extending on a companion paper in this colloquium, the dispersion, ignition and combustion characteristics of aluminum particle clouds is investigated numerically behind reflected shock waves. It is observed that a higher proportion of the Al cloud by mass burns for a higher initial cloud concentration. Vorticity from the cloud wake and from that deposited by the reflected shock cause the particle cloud to convolute, and this effect is particularly very significant for higher concentration clouds. Faster ignition delay times and higher overall Al burning by mass are observed for stronger incident shock Mach numbers due to the consequent hotter gas temperatures behind the reflected shock wave. A mass-weighted ignition parameter is introduced in this study and is identified to be particularly useful to determine overall cloud ignition trends.

1 Introduction

Aluminum particle clouds have been widely studied by the research community due to its high energy content, making it useful for many engineering applications such as in solid propellants, explosives, fuel systems, and the like. Experiments on the combustion of individual aluminum particles was undertaken by Friedman & Macek [1], investigating the effects of ambient gas temperature, oxygen content, and aluminum particle size and they obtained an empirical correlation for the ignition delay time conforming to the classical d_p^2 law, where d_p is the particle diameter. Later, experiments on aluminum particles at higher pressures were undertaken by Belyaev et al. [2], and they concluded: the burning time is independent of the pressure and temperature but strongly depends on the oxidizing medium; the ignition delay time is insensitive to the composition of the oxidizer and pressure, but depends on the temperature. Gurevich et al. [3] obtained an empirical relation for the limiting temperature for the ignition of aluminum particles as a function of particle size, oxidizer concentration and gas temperature. All these early studies focused on ignition of aluminum particles at stagnant or very low speed conditions.

Later, interest on aluminum particle combustion in high-speed environments also gained attention. Experimental studies on the ignition of aluminum particle clouds behind reflected shock waves were carried out by Boiko et al. [4, 5], and they demonstrated that the combustion characteristics of aluminum depend on the particle size, cloud density as well as shock strength. With the advent of computing power, simulations of aluminum particle cloud ignition behind explosions and/or shock waves is gaining increased interest, as is evidenced by the studies of Kuhl et al. [6, 7] and Balakrishnan et al. [8, 9]. While the former studies employ Eulerian approaches, the latter explores Lagrangian tracking of particles in post-detonation flow-fields. These studies primarily investigate, inter alia, the role of turbulent mixing on the ignition of aluminum particle clouds. In a companion paper in this colloquium [10], the Kuhl & Boiko [11] empirical Al ignition model is employed to investigate the ignition characteristics behind explosive blast waves. The same methodology is employed in this study to investigate the ignition characteristics behind reflected shock waves. This ignition model incorporates experimental data from the Boiko experiments [4, 5].

This paper is organized as follows: Section 2 presents the numerical formulation used in the present study; Section 3 summarizes the results and discussions; the main conclusions of this study are summarized in Section 4.

2 Formulation

The two-phase gasdynamic model of Nigmatulin [12] is considered for the current simulations, assuming both the gas and solid phases to be governed by separate continuum laws. Source terms for mass, momentum and energy

Table 1: Initial conditions for the different cases considered in this study

Case	ρ_s, g/m^3	M_o	T_g behind incident shock, K	T_g behind reflected shock, K
1	200	4	1110	1920
2	100	4	1110	1920
3	50	4	1110	1920
4	100	3.5	925	1590
5	100	3.8	1030	1780

account for the interaction between the two phases. For brevity, these equations are not discussed here, but can be found elsewhere [6, 7]. The ignition delay time, t_{ign}, that appears in the model is obtained as follows:

$$\frac{1}{t_{ign}(T_g)} = A_{Kuhl-Boiko}\, exp\left(\frac{-E_{a,Kuhl-Boiko}}{RT_g}\right), \quad T_g \leq 2500K;$$

$$\frac{1}{t_{ign}(T_g)} = A\, d_p^2\, exp\left(\frac{-E_a}{RT_g}\right), \quad T_g > 2500K, \tag{1}$$

where d_p is the particle diameter. The above constants are computed based on re-shocked aluminum ignition experiments performed by Boiko et al. [4, 5] for ambient gas temperatures $\leq$ 2500 K, and are determined to be $A_{Kuhl-Boiko} = 6.25 \cdot 10^{10}$ sec^{-1} and $E_{a,Kuhl-Boiko} = 60$ KCal/mol for flake aluminum of size 4–6 μm [11]. For higher ambient gas temperatures, $E_a = 22.8$ KCal/mol based on Roberts et al. [13] is used, and A is assumed to take the value $1 \cdot 10^8$ sec^{-1}. An ignition temperature of 1785 K is assumed; thus, the particle temperature must be higher than this temperature as well as the ignition variable $f \geq 1$ in order for mass transfer to occur.

High-resolution upwind methods that are higher-order generalizations of Godunov's method are employed to solve the governing equations using efficient Riemann solvers for the gas [14, 15] and particle phases [16]. Local Adaptive Mesh Refinement (AMR) [17] is used to resolve the finer scales in the mixing zone, and the overall simulation strategy is consistent with the ILES approach [18]. Many recent studies [6, 7, 10] have demonstrated the efficacy and robustness of this methodology.

3   Preliminary Results and Discussion

Simulations are carried out to investigate the ignition characteristics of spherical aluminum particle clouds behind reflected shock waves in air. A 3.2 m $\times$ 0.4 m $\times$ 0.4 m shock tube is considered with an inflow at $x = 0$ and slip walls on all other 5 walls. A shock wave is initialized at $x = 0.5$ m, with the region $0 \leq x \leq 0.5$ initialized with the Rankine-Hugoniot jump conditions for air, and the region $x > 0.5$ initialized with static air at 0.1 bar and 293 K. A spherical particle cloud 5 cm in radius, comprising of 4–6 μm diameter Al flakes, is injected at the $x = 2.75$ m location at 2.25 msec; this corresponds to a time instant after the passage of the incident shock wave, but before the shock reflection at the end wall ($x = 3.2$ m). A similar experimental setup was considered by Boiko & Poplavski [5]. Different particle cloud densities, ρ_s, in the range 50–200 g/m^3 are of interest and the particle cloud is initialized with the desired ρ_s superimposed with a 5% random perturbation. A 512$\times$64$\times$64 base grid with three levels of adaptive refinements corresponding to refinement ratios of 2 per level is considered for the present analysis.

The flow behind the incident shock wave accelerates the particle cloud, causing it to disperse towards the end wall. Subsequently, the shock wave reflects from the end wall, and then interacts with the particle cloud, dragging the particle cloud wake into the cloud. At the same time, the high temperature behind the reflected shock wave ignites the particle cloud. Vorticity from the reflected shock further mixes the particle cloud, giving it a distorted shape. The primary focus of this study is to investigate the effect of particle cloud density and incident shock Mach number on the ignition characteristics and the subsequent dispersion of the cloud. Table 1 summarizes the key initial conditions including the initial cloud densities (ρ_s), incident shock wave Mach number (M_o), gas temperatures (T_g) behind the incident and reflected shocks, for the different cases considered in this study.

First, we explore the effect of initial cloud density, ρ_s, for the same M_o, i.e., Cases 1–3 in Table 1. Based on the experiments of Boiko et al. [4, 5], above a certain ρ_s threshold, the ignition characteristics do not depend on ρ_s; cloud ignition was not reported to occur below this threshold. Unlike most other Al ignition/combustion models in the literature, ours takes this factor into account (explained in [10]), and therefore we expect sensitivity of the results to ρ_s. Analysis shows that a higher ρ_s results in a larger wake behind the particle cloud with stronger

vortices. As the reflected shock drags this wake into the particle cloud, this causes the latter to also convolute, thereby increasing the overall surface area of the particle cloud; for the present setup, the reflected shock wave starts to interact with the particle cloud around 2.5 msec. Since the wake vortices are more pronounced for higher ρ_s, the cloud shape is more convoluted. This is illustrated in Fig. 1 for Case 1 and Fig. 2 for Case 3, showing the varying cloud shapes for different ρ_s. Since the effect of ρ_s is inherent in our Al evaporation model (see [10, 11] for further details), Case 1 results in higher burning trends than Case 3. The exact amount of Al remaining is quantified in Fig. 3 with the presentation of the absolute mass of solid Al, m_{Al}, remaining with time and the normalized mass (normalized with the initial mass, m_{Al}^o). Whereas the ignition time delay is nearly identical for different ρ_s, the late time amount of Al that remains with time is sensitive to ρ_s. For a lower initial ρ_s, at later times many regions of the particle cloud tend to have a concentration lower than the chosen threshold value. Thus, this study identifies that cloud concentration, ρ_s, does indeed play a critical role both in the dispersion as well as ignition/combustion characteristics of the cloud.
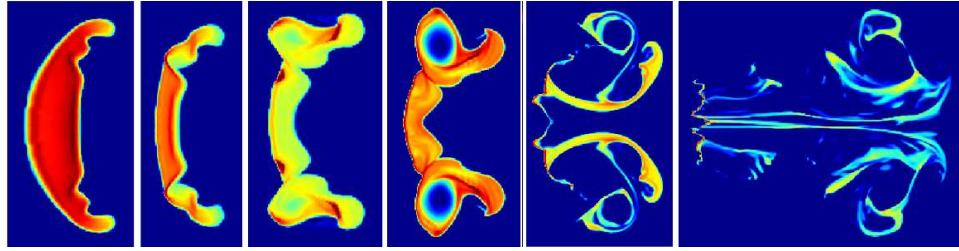
Figure 1: $\log(\rho_s)$ at 2.57, 2.6, 2.68, 2.78, 3.58 and 5.38 msec for Case 1. (Red is high, green is medium and blue is low.)
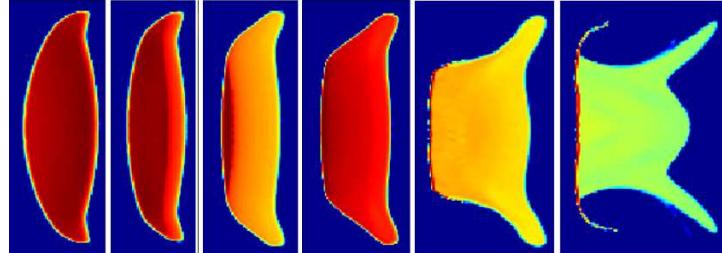
Figure 2: $\log(\rho_s)$ at 2.57, 2.6, 2.68, 2.78, 3.58 and 5.38 msec for Case 3. (Red is high, green is medium and blue is low.)
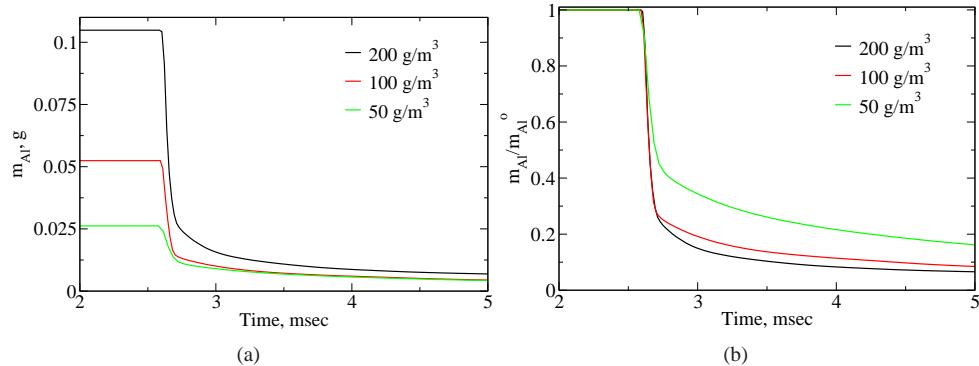
Figure 3: Mass of solid Al (m_{Al}) remaining with time for Cases 1–3: (a) absolute mass in grams; (b) normalized mass.

As the late time particle cloud shape is sensitive to initial ρ_s, the regions of enhanced burning encountered in the cloud will not be uniform for the different cases considered. Thus, it is of preponderant interest to identify the burning regions for different cloud concentrations at late times. To this end, the gas temperature, T_g and the oxidizer mass fraction are of interest and are studied here qualitatively. T_g is shown in Fig. 4 (a) & (b) at 5.38 msec for Cases 1 and 3, respectively; as evident, the overall burning zone is more elongated for Case 1, with

the burning being primarily concentrated at the tips of the zone. For Case 3, however, the burning zone is less distorted and stays concentrated primarily in the leading edge. A comparison of the oxidizer mass fractions for these two cases at the same time instant is presented in Fig. 5. As expected, a shortage of oxidizer—identified by the blue regions—is encountered in the hotter regions. It is interesting to also note that the oxidizer concentration reaches zero for Case 1, albeit not for Case 3. Due to the higher Al mass in Case 1, pockets of oxidizer are rapidly consumed completely, ensuing in competition for oxidizer in the vicinity of these regions.

Furthermore, the post-reshock cloud shape is reminiscent of shocked dense gas bubble shapes reported in past experiments by Haas & Strutevant [19], presented in Fig. 5 (c). This means that the particle cloud in some sense acts as a dense gas; however, its velocity and temperature are not in equilibrium with the local gas and therefore they are not identical. Thus, some of the vortex dynamics theories applied in the past for shocked dense gases can perhaps be extended to particle clouds as well to explain the late time dispersion trends.
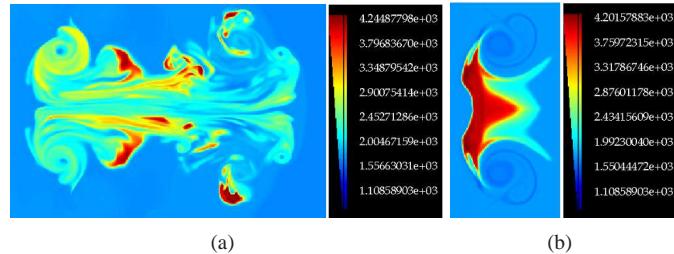
Figure 4: Gas temperature in Kelvin at 5.38 msec for a Mach 4 incident shock: (a) Case 1 and (b) Case 3.
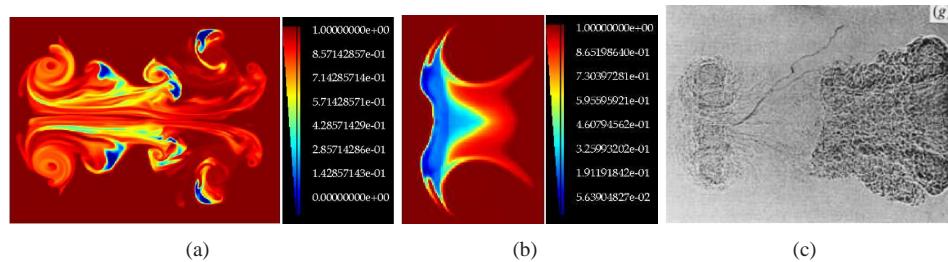
Figure 5: Oxidizer mass fraction at 5.38 msec for a Mach 4 incident shock: (a) Case 1; (b) Case 3; (c) gas bubble shape from [19].

Next, we investigate the effect of incident shock Mach number, M_o, i.e., Cases 2, 4 & 5 in Table 1. Analysis shows that the Al cloud does not ignite for the $M_o = 3.5$ cloud as the gas temperature behind the reflected shock is not hot enough. The ignition variable, f, is presented in Fig. 6 at 5.3 msec, and shows that the cloud shapes are very different due to the different amounts of vorticity deposited in the respective clouds. The mass of Al remaining is shown in Fig. 7 (a) and a stronger shock gives rise to not only faster ignition, but also enhanced burning trends by mass due to the higher gas temperatures behind the reflected shock. The mass-averaged Al particle temperature, $T_{s,ave}$, is presented in Fig. 7 (b) and reveals three heating regions—that due to the flow behind the incident shock at early times, followed by due to the reflected shock, and lastly due to Al combustion. It is interesting to note that Case 1 attains peak $T_{s,ave} \sim 400$ K lower than the other burning cases, even though this corresponds to higher overall Al burning trends. This is because significantly higher cloud mass for Case 1 inevitably results in competition for heat in many regions of the particle cloud around 2.75 msec, due to which the energy release from the burning particles gets distributed over a wider region. Around 3.5 msec, $T_{s,ave}$ for Case 1 nearly flattens out unlike the other cases, demonstrating that Al burning sustains itself for a longer time for this case.

Very often, when a cloud of particles ignite and burn, some regions of the cloud may ignite earlier than others. To this end, it is also of interest to determine a mass-weighted ignition paramter that can determine the global ignition characteristics of the cloud. This quantitity is computed as $f_{MW} = \int \rho_s \cdot f \, dV$, integrated over the entire simulation domain. The variation of this parameter for the different cases under study here are presented in Fig. 8 to investigate the (a) effect of ρ_s and (b) effect of M_o. From Fig. 8 (a), the initial rise occurs at the same time (2.5 msec) for the three cases, i.e., the time when the reflected shock reaches the cloud. However, the peak values and the subsequent decay rates are different due to the different amounts of burning experienced in the three different clouds. The shape of this parameter is similar to photodiode signals of the burning cloud presented by experimentalists, see for instance [13]. It is interesting to note that for the $\rho_s = 200$ g/m^3 cloud, the burning occurs

(a)   (b)   (c)
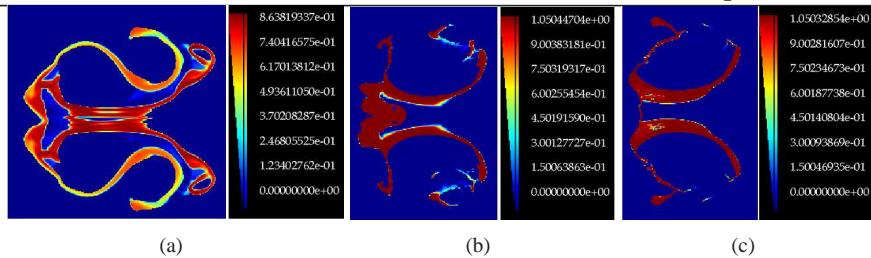
Figure 6: Effect of Mach number on ignition characteristics: ignition variable f for 100 g/m^3 cloud at 5.3 msec corresponding to (a) Mach 3.5; (b) Mach 3.8; (c) Mach 4.

(a)   (b)
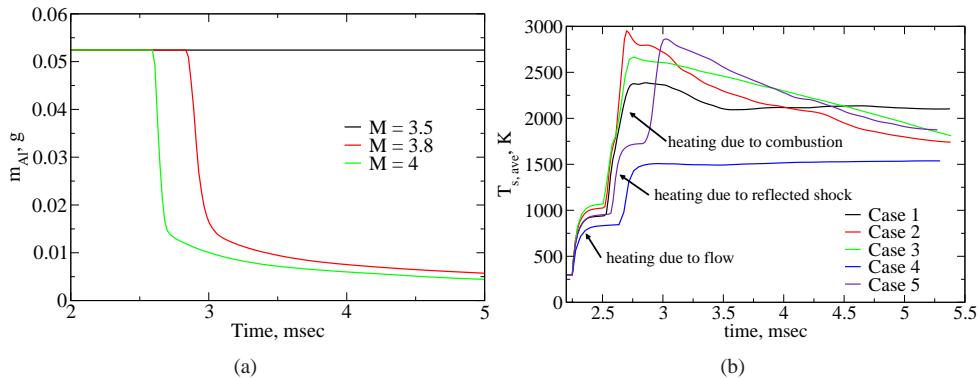
Figure 7: (a) Effect of Mach number on burning characteristics (Cases 2, 4 & 5); (b) mass-averaged Al temperature, $T_{s,ave}$.

with a minor 'kink' in the profile as indicated by the arrow in Fig. 8 (a). This is presumably due to the enhanced mixing encountered due to the higher vorticity levels, which can ignite more regions of the particle cloud around this time instant (2.75 msec).

This mass-weighted ignition parameter for different M_o are presented in Fig. 8 (b) corresponding to initial cloud densities of 100 g/m^3 (Cases 2, 4 & 5 in Table 1). The cloud does not ignite for M_o = 3.5 as the gas temperatures behind the reflected shock are not hot enough, resulting in an ever-increasing trend. M_o = 4 ignites the cloud earlier than M_o = 3.8; however, the peak values of this mass-weighted ignition variable are reversed. This is because since ignition is delayed for M_o = 3.8 compared with M_o = 4, the total mass of Al remaining at the subsequent times ($\sim$ 3–4 msec) is greater for the former, thereby resulting in the higher peak. In addition, due to the delayed ignition, more regions of the particle cloud experience higher f; consequently, higher values of this parameter are seen for M_o = 3.8.

The profiles for f_{MW} are reminiscent of photodiode voltage signals typically used by experimental researchers to obtain burn times of Al particles. For instance, Roberts et al. [13] used the time duration between the 50% of the peak voltage during the rise and fall as the burn time of particles. Using a similar analogy for f_{MW}, we obtain the burn time of the 4—6 μm flake Al as $\sim$ 250 μsec, which is comparable to the burn times obtained for spherical Al particles of a similar size under similar conditions [20]. Thus, by using experimental ignition delay times in our ignition model, we can also compute the burn times of Al particles from f_{MW} profiles. More studies along these lines will be conducted in the future.

4   Conclusions

The ignition and combustion characteristics of aluminum particle clouds behind reflected shock waves was investigated using a robust, adaptive, two-phase simulation strategy. A higher initial particle concentration of the cloud leads to enhanced overall Al burning by mass. Furthermore, vorticity from the wake as well as from the shock deposition convolutes the particle cloud and this effect is significant for higher concentration particle clouds, leading to an elongated cloud shape at later times. Stronger incident Mach numbers result in faster ignition delay times as well has higher overall burning trends by mass due to the higher gas temperatures encountered behind the cloud.
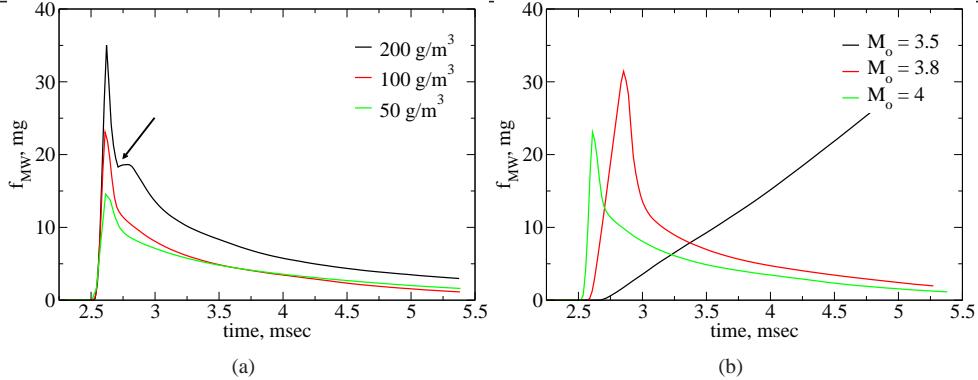
Figure 8: Mass-weighted ignition variable f_{MW} variation with time: (a) effect of ρ_s; (b) effect of M_o.

In addition, the mass-weighted ignition parameter is identified as a useful parameter to investigate global cloud ignition characteristics.

5   Acknowledgments

References

[1] R. Friedman and A. Macek, *Ignition and Combustion of Aluminum Particles in Hot Ambient Gases*, Combustion and Flame 6 (1962), pp. 9–19.

[2] A. F. Belyaev, Yu. V. Frolov and A. I. Korotkov, *Combustion and Ignition of Particles of Finely Dispersed Aluminum*, Combustion, Explosion and Shock Waves 4(3) (1968), pp. 323–329.

[3] M. A. Gurevich, K. I. Lapkina and E. S. Ozerov, *Ignition Limits of Aluminum Particles*, Combustion, Explosion and Shock Waves 6(2) (1970), pp. 154–157.

[4] V. M. Boiko, V. V. Lotov and A. N. Papyrin, *Ignition of Gas Suspensions of Metallic Powders in Reflected Shock Waves*, Combustion, Explosion and Shock Waves 25(2) (1989), pp. 193–199.

[5] V. M. Boiko and S. V. Poplavski, *Self-Ignition and Ignition of Aluminum Powders in Shock Waves*, Shock Waves 11(4) (2002), pp. 289–295.

[6] A. L. Kuhl, J. B. Bell and V. E. Beckner, *Heterogeneous Continuum Model of Aluminum Particle Combustion in Explosions*, Combustion, Explosion and Shock Waves 46(4) (2010), pp. 433–448.

[7] A. L. Kuhl, J. B. Bell and V. E. Beckner, *Gasdynamic Model of Turbulent Combustion in TNT Explosions*, 33rd International Combustion Symposium, Beijing, China, August 1–6 (2010).

[8] K. Balakrishnan, and S. Menon, *On the Role of Ambient Reactive Particles in the Mixing and Afterburn Behind Explosive Blast Waves*, Combust. Sci. and Tech. 182(2) (2010), pp. 186–214.

[9] K. Balakrishnan, and S. Menon, *On Turbulent Chemical Explosions Into Dilute Aluminum Particle Clouds*, Combust. Theo. and Model. 14(4) (2010), pp. 583–617.

[10] K. Balakrishnan, A. L. Kuhl, J. B. Bell and V. E. Beckner, *An Empirical Model for the Ignition of Aluminum Particle Clouds Behind Blast Waves*, ICDERS, July 24-29 (2011), Irvine, CA.

[11] A. L. Kuhl and V. M. Boiko, *Ignition of Aluminum Particles and Clouds*, 41st Int. Conf. of ICT Energetic Materials, June 29–July 2 (2010), Karlstruhe, Germany.

[12] R. I. Nigmatulin, *Dynamics of Multiphase Media, Part I*, Hemisphere, New York (1991).

[13] T. A. Roberts, R. L. Burton and H. Krier, *Ignition and Combustion of Aluminum/Magnesium Alloy Particles in O_2 at High Pressures*, Combustion and Flame 92 (1993), pp. 125–143.

[14] J. B. Bell, P. Colella and A. Trangenstein, *Higher Order Godunov Methods for General Systems of Hyperbolic Conservation Laws*, J. Comput. Phys. 82(2) (1989), pp. 362–397.

[15] P. Colella, *Multidimensional Upwind Methods for Hyperbolic Conservation Laws*, J. Comput. Phys. 87 (1990), pp. 171–200.

[16] P. Collins, R. E. Ferguson, K. Y. Chien, A. L. Kuhl, J. Krispin and H. M. Glaz, *Simulation of Shock-Induced Dusty Gas Flows Using Various Models*, AIAA Fluid Dynamics Conference (1994), AIAA 94-2309.

[17] M. J. Berger and P. Colella, *Local Adaptive Mesh Refinement for Shock Hydrodynamics*, J. Comput. Phys. 82(1) (1989), pp. 64–84.

[18] F. F. Grinstein, L. G. Margolin and W. J. Rider (Editors), *Implicit Large-Eddy Simulation: Computing Turbulent Fluid Dynamics*, Cambridge Univ. Press, Cambridge, UK (2007).

[19] J. F. Haas and B. Strutevant, *Interaction of Weak Shock Waves with Cylindrical and Spherical Gas Inhomogeneities*, J. Fluid Mech. 181 (1987), pp. 41–76.

[20] P. Lynch, H. Krier and N. Glumac, *A Correlation for Burn Time of Aluminum Particles in the Transition Regime*, Proc. Combust. Inst. 32 (2009), pp. 1887–1893.